High resolution, consistent navigation and 3D optical reconstructions from AUVs using magnetic compasses and pressure-based depth sensors

Michael V. Jakuba, Oscar Pizarro, Stefan B. Williams
Australian Centre for Field Robotics
University of Sydney, Sydney NSW 2006 Australia
{m.jakuba,o.pizarro,stefanw}@acfr.usyd.edu.au

***Abstract*— Benthic imaging AUVs can deliver down-looking imagery with consistent altitude and illumination. These images are well suited to image matching routines that form the basis for mosaicking, vision-based Simultaneous Localisation and Mapping (SLAM) and 3D visual reconstructions. We show how these same visual constraints can be used to (1) improve the real time dead-reckoning accuracy of AUVs equipped with magnetic compasses and (2) to quantify the accuracy of various corrections applied to measured pressure to determine vehicle depth. We present results from full coverage optical imaging surveys conducted in the field by our AUV to illustrate the impact of these refinements on the ability of the vehicle to successfully complete its missions and the quality of the resulting seafloor models.**

I. Introduction

Benthic acoustic and optical imaging AUVs have become effective complements to traditional survey methods; however their use has been largely restricted to exploratory missions at depths and in regions difficult to map at high resolution by other means [1], [2], [3]. To address pressing questions about the effect of climate change and direct anthropogenic impacts on coastal and deep sea benthic ecology, AUVs must start operating in a monitoring capacity. So far, these efforts have largely focused on physical oceanographic [4] or pelagic phenomena [5] but benthic imaging AUVs can now rapidly and cost-effectively deliver high resolution, accurately geo-referenced, and precisely targeted optical and acoustic imagery. This makes AUVs ideally suited to the kinds of repeat surveys that will be necessary to monitor changes in the benthos, particularly beyond diver depths.

Full coverage grid photomosaics cover a large area relative to the footprint of a single constituent image, allowing researchers to register and cross-compare data from separate dives in post-processing with a reduced need for accurate real-time geo-referencing. If individual images or linear transects were to be compared, cm-scale real time control and geo-referenced navigation would be required between dives. Full coverage areal photomosaicking reduces this requirement to cm-scale real-time relative navigation and control during individual dives.

Full coverage optical imaging surveys that are tens to a few hundred meters on a side composed of tightly O(1 m) spaced parallel tracklines are currently feasible using vehicles equipped with a navigation suite including a Doppler velocity log (DVL) and a high end inertial navigation system

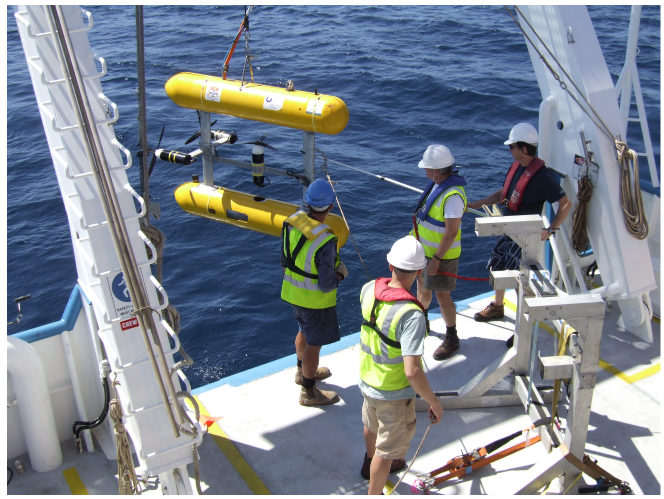

Fig. 1. The Australian Centre for Field Robotics' benthic imaging AUV, *Sirius*, being recovered during survey operations at Scott Reef, Western Australia. Photo by Dr. Duncan Mercer.

(INS). Since an INS can represent a substantial portion of the capital costs of a small or mid sized AUVs, scientific applications that rely on an AUV with an INS are less likely to become widespread, particularly if multiple vehicles are needed.

Mid-range navigation suites include a DVL but typically rely on a magnetic compass or magnetometer as a heading reference. These instruments are orders of magnitude cheaper than an INS but are sensitive to the magnetic signature of the rest of the vehicle [6], which can introduce distortions of several degrees into the heading estimate. Even when special care goes into soft and hard iron calibration, persistent heading-dependent errors of O(1 deg) are possible. While adequate to perform linear transects or broader acoustic surveys (particularly when aided by acoustic positioning from LBL or USBL), the magnitude of these errors makes an intended 'mow the lawn' pattern with reciprocal, closely spaced, parallel tracklines unlikely to succeed. An error of 1 degree over a 100 m trackline represents approximately a 2 m arc, which, depending on the sign of the error implies that tracklines can 'accordion' out with unintended gaps between tracklines or 'figure 8' with reduced coverage and excessive overlap. Figure 2 shows two dives completed with our AUV that illustrate these patterns and that provided the motivation

978-1-4244-5222-4/10/$26.00 ©2010 IEEE

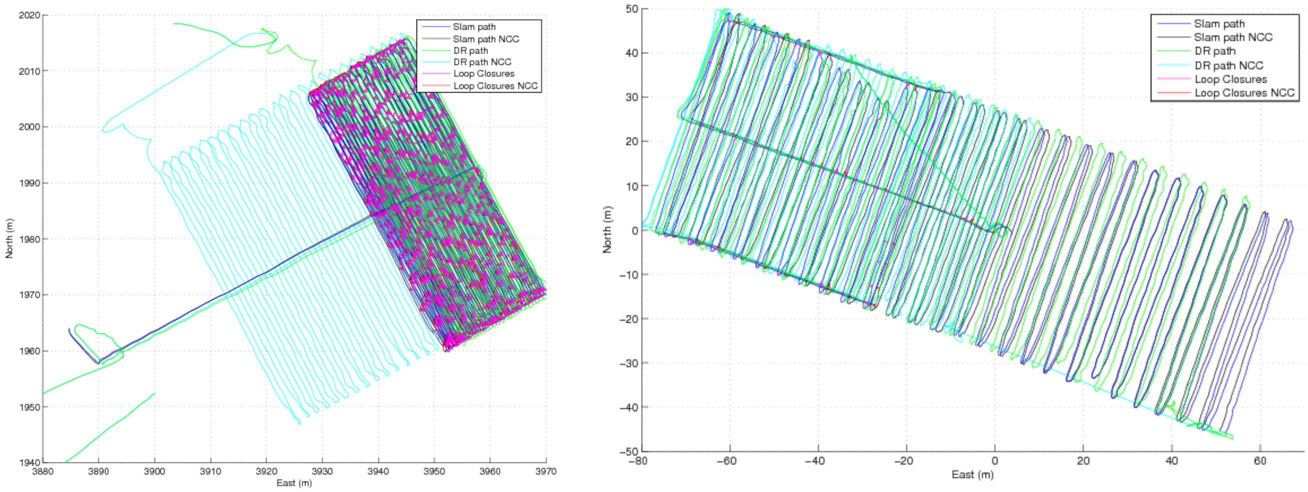

(a) (b)

Fig. 2. Estimated vehicle trajectories for attempted full-coverage surveys with an imperfectly calibrated compass (No Compass Correction, NCC): (a) ‘figure 8’ compression on reciprocal tracklines; (b) ‘accordion’ expansion on reciprocal tracklines. These distortions are not apparent underwater in real time (DR path), and become apparent only when GPS data are fused into the navigation estimate after surfacing. Post-processed navigation incorporating visual loop-closures (SLAM path) confirmed the distortions.

for this study.

The class of AUV used in this study has been designed specifically for relatively low speed, high resolution imaging and is passively stable in pitch and roll. Our submersible (Fig. 1) is equipped with a full suite of oceanographic sensors including a high resolution stereo camera pair and strobes, multibeam sonar, a depth sensor, DVL including a compass with integrated roll and pitch sensors, and Ultra Short Baseline acoustic positioning system (USBL). Passive stability in pitch and roll not only improves image quality, but also substantially reduces the complexity of compass calibration. Out-of plane distortions become irrelevant and calibration can be conducted in situ. This fact is important logistically since it is often difficult to find a a location free of distortions to the Earth’s magnetic field on a steel ship or dock.

It is possible to recover 3D structure and vehicle pose estimates that are consistent with that structure by using visual SLAM to optimally fuse uncertain navigation estimates and visual observations [7] [8]. Cameras are capable of high resolution observations such that if the same scene is imaged from different headings, these will be recovered with high precision though without any notion of true North. We show that it is possible to derive a heading-dependent correction to the magnetic compass using visual data and that this correction has a cyclic form that can be approximated and easily identified by a Fourier series expansion. This type of correction was used in post-processing to generate improved navigation estimates in [9] and [10] but this is the first time it has been used to enable a compass-equipped AUV to perform dense visual coverage of a seafloor patch of approximately 50 m x 75 m with 50 parallel tracklines.

We demonstrate that visually-derived relative pose constraints can also reveal the existence of false depth variations. This allows us to assess the quality of any corrections applied and to quantify the extent of remaining error. Tidal corrections in particular are important for deployments lasting several hours.

This paper is organised as follows. Section II provides relevant background on visually-derived relative pose constraints, underwater visually-augmented simultaneous localisation and mapping (SLAM), and solid-state magnetic compass calibration. Section III reports our methods for in situ compass calibration and for depth correction. Section IV shows results of this work applied in the field on a research cruise to Scott Reef, Western Australia, illustrating the improvements in navigation achievable with a relatively low cost navigation system. Finally, Section V presents conclusions and discusses directions for future work in this area.

II. Background

A. *Visually-Derived Relative Pose*

Determining relative pose between views of the same scene hinges on identifying corresponding points in each view. For wide-baseline imaging, such as that corresponding to loop closures or motion comparable to the range to the scene, appearance can change substantially and feature matching is typically employed over correlation-based approaches. Several automatic wide baseline 2D feature detectors and descriptors have been proposed with the Scale Invariant Feature Transform (SIFT) [11] being widely used for its discriminative power and invariance to rotations and changes in scale. The results presented in this paper use SIFT features to recognize loop closures.

Several approaches can be used to derive relative pose estimates from visual data. Most underwater vehicle systems use monocular cameras, in which case under general motion of the camera (and vehicle) and structure in the scene it is possible to recover a 5DOF relative pose, corresponding to the change in orientation (3DOF) and the direction of motion (2DOF). The magnitude of the displacement and the scale of the triangulated scene is lost in the image formation process. Land based computer vision established the machinery for robust estimation of relative pose relying on epipolar constraints [12]. Typically an uncalibrated camera is assumed which is reasonable when the camera is the only instrument being used. However, underwater vehicles are typically pose-instrumented, and these additional pose measurements can aid the motion estimate if the camera is calibrated [9]. In this case, scale is imposed by the DVL or known reference points.

A stereo vision system offers the advantage of a known baseline, resulting in a 6DOF estimate of relative pose between two stereo pair views of a common scene. Given that the observations correspond to feature locations on the imaging planes, the maximum likelihood (ML) solution involves minimizing the reprojection error on the imaging plane between observed 2D features and the projection of the modelled 3D structure onto the modelled cameras by adjusting the parameters describing camera poses and 3D scene features locations. The stereo baseline can be held fixed in this case. Alternatively, the 3D structure resulting from triangulating feature points in each stereo pair can be registered, which is computationally simpler. We use a robust form of registration of 3D points that accounts for uncertainty in the triangulation and approaches the ML solution but is significantly faster to calculate [13].

B. *Visually-Augmented Navigation*

Navigation underwater is challenging because electromagnetic signals attenuate rapidly in seawater. Absolute position estimates such as those provided by GPS are therefore not available. Simultaneous Localisation and Mapping (SLAM) is the process of concurrently building a map of the environment and using this map to obtain estimates of the location of the vehicle. The SLAM algorithm has seen a considerable amount of interest from the mobile robotics community as a tool to enable fully autonomous navigation [14], [15]. We have previously reported on our stereo based Simultaneous Localisation and Mapping and dense scene reconstruction suitable for creating detailed maps of seafloor survey sites [13], [16]. These approaches, based on Visual Augmented Navigation (VAN) techniques [17], efficiently manage the complexity of recovering the state estimate and covariance matrix in a VAN framework. This has allowed these algorithms to run on significantly larger mapping problems than was previously feasible.

Although it is possible to correct for dead reckoning drift using SLAM techniques following recovery of the vehicle, the vehicle itself must be able to complete the designated missions while it is underway. While the SLAM techniques themselves are efficient and can handle many tens of thousands of estimated vehicle poses, the lighting correction and feature extraction steps currently remain slower than real time. Presently we rely on dead-reckoning to provide sufficiently accurate real time navigation for full coverage optical surveys. For a mid-range navigation suite consisting of a DVL, inclinometer and magnetic compass, such surveys require sub-degree heading accuracy from the compass if distortion like that evident in Fig. 2 is to be avoided.

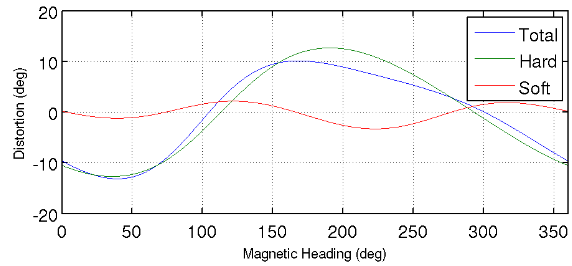

Fig. 3. Heading distortion in the horizontal plane resulting from the hard and soft iron characteristics of a notional vehicle.

Loop closures derived from visual constraints provide near-groundtruth relative navigation on the scale of individual surveys provided these contain sufficient reobservations of the same terrain. In this paper we use the SLAM result from a calibration dive to compute a compass correction that provides the requisite accuracy. Identification of heading bias allows realistic heading measurement noise to be used in the SLAM filter, rather than an inflated noise level which is the naive strategy to ensure that navigation uncertainty will be large enough to include matching images in the unmodelled bias case. Accounting for heading biases also improves SLAM running time since a reduced number of images must be tested for loop-closures.

C. *Magnetic Compass Calibration*

Solid state magnetic flux-gate compasses of the type commonly employed for low-cost autonomous platform navigation measure the three-dimensional vector components of the incident magnetic field in the frame of the vehicle, ${}^{v}\mathbf{h}$. Provided with the remaining orientations of the sensor relative to the gravity vector (e.g., the two tilts from an inclinometer, or equivalently pitch and roll), these vehicle-frame measurements can be rotated into local-level components of the magnetic field ${}^{l}\mathbf{h} = {}^{l}_{v}\mathbf{R}\,{}^{v}\mathbf{h}$. A heading estimate $\hat{\psi}$ may then computed according to

$$\hat{\psi} = \operatorname{atan2}\Big(-{}^{l}h^{(2)}, {}^{l}h^{(1)}\Big) \ , \tag{1}$$

where the parenthesized superscripts denote components of the vector.

The heading computed this way will be accurate within the limits of the inclinometer, temperature effects, A/D resolution, and distortions to the Earth's magnetic field resulting from the magnetic signature of the vehicle itself. The resulting error budget for this kind of compass, properly calibrated for magnetic distortions, adds up to approximately one degree [6]. Compass calibration is the procedure of removing the effects of a vehicle's magnetic signature. A vehicle's magnetic signature can be decomposed into two

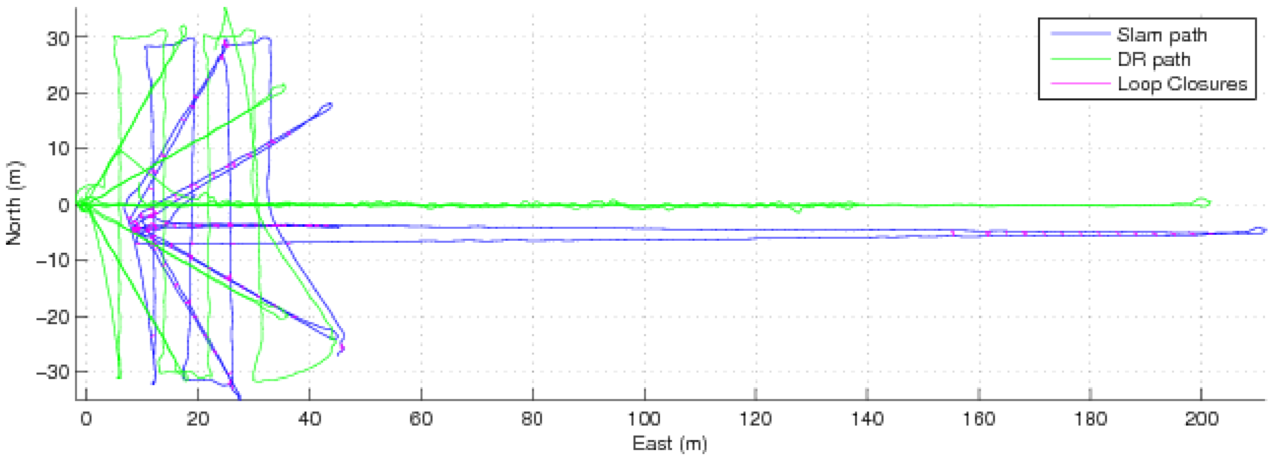

Fig. 4. Navigation check dive. Compass headings measured in real time and used to generate the dead reckoned track (green) are compared with headings from the SLAM navigation estimate (blue). The magenta lines designate loop closures between poses.

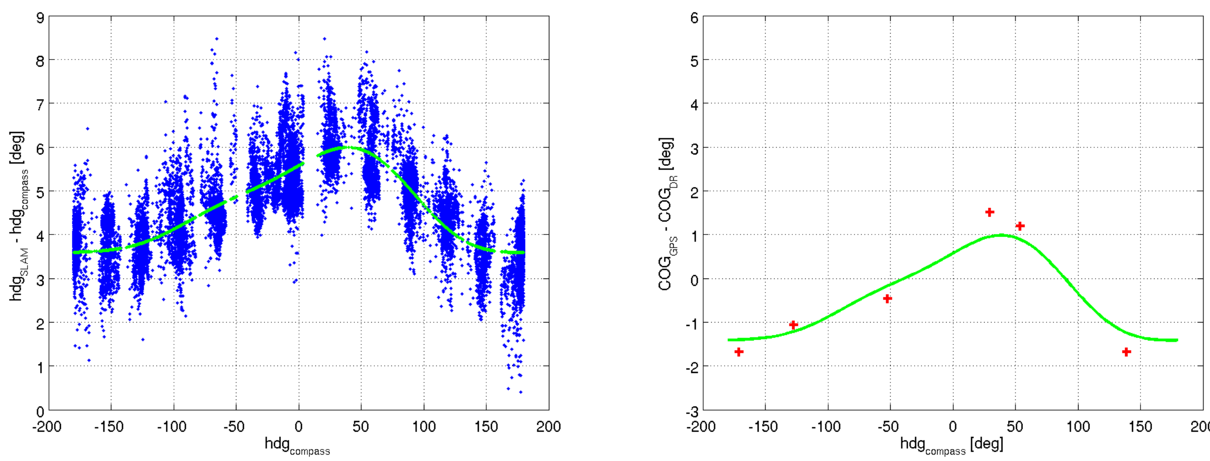

(a)

(b)

Fig. 5. (a) Compass distortion based on the differences between estimated headings from the SLAM solution and the compass readings for a calibration dive that imaged the same small area from multiple headings. Data points (blue) are used to derive a Fourier series approximation using the first three harmonics (green). (b) Least squares fit of the correction curve derived from the SLAM data to GPS course-made-good derived from long subsurface transects.

components, a hard-iron offset due to the magnetic field of permanently magnetized materials and a soft-iron component due to induced magnetism in materials that become magnetized in an orientation-dependent way when exposed to an incident magnetic field.

The resulting field measured in a vehicle-fixed frame consists of a distorted version of the Earth's field $\mathbf{h_e}$ plus a constant hard iron distortion $\mathbf{h_{hard}}$:

$$ {}^{v}\mathbf{h} = (\mathbf{H}_{soft} + \mathbf{I})\, {}^{v}\mathbf{h_e} + {}^{v}\mathbf{h_{hard}} \,. \tag{2} $$

Here $\mathbf{H}_{soft}$ denotes a 3×3 matrix of scaling and coupling coefficients that model the soft-iron properties of the vehicle [18]. Upon rotation into the level frame, the measured field is

$$ {}^{l}\hat{\mathbf{h_e}} = {}^{l}_{v}\mathbf{R}(\mathbf{H}_{soft} + \mathbf{I})\, {}^{v}_{l}\mathbf{R}\, {}^{l}\mathbf{h_e} + {}^{l}_{v}\mathbf{R}\, {}^{v}\mathbf{h_{hard}} \,. \tag{3} $$

The portion of the magnetic field that represents distortions is given by

$$ {}^{l}\tilde{\mathbf{h_e}} = {}^{l}_{v}\mathbf{R}\mathbf{H_{soft}}\, {}^{v}_{l}\mathbf{R}\, {}^{l}\mathbf{h_e} + {}^{l}_{v}\mathbf{R}\, {}^{v}\mathbf{h_{hard}} \,. \tag{4} $$

In three dimensions the total measured magnetic field in the vehicle frame is an ellipsoid whose eccentricity depends on $\mathbf{H_{soft}}$ with an offset from the origin equal to $\mathbf{h_{hard}}$. Without any distortion the field would describe a sphere centered at the origin. Manufacturers usually provide calibration routines designed to sample the three-dimensional magnetic field around the compass and identify this distortion [6]. These routines typically involve orienting the vehicle in various known directions or spinning it at various tilts. The results can then be used to compensate the component measurements prior to using (1) to compute heading. Alternatively, a correction curve can be applied to computed heading (Fig. 3). The appearance of the rotation ${}^{l}_{v}\mathbf{R}$ in (4) implies the accuracy of the correction will suffer for out-of-plane tilts.

A practical issue arises with these procedures when applied to AUV operations: it may not be possible to arbitrarily orient vehicles weighing more than a few tens of kilograms in an area free of magnetic disturbances. This issue is particularly acute at sea when on board a steel ship, with little recourse when a calibration performed prior to commencing fieldwork proves inadequate in the field.

D. Depth from Pressure

In contrast to the more difficult horizontal-plane positioning problem, underwater navigation in the vertical dimension benefits from the availability of pressure as an absolute reference. Pressure sensors in common use can attain accuracies of 0.1–0.01% of their depth rating [19]. However, the combined effect of tides, waves, atmospheric pressure variations, persistent on- or offshore winds along coasts, and variations in seawater density can compromise the accuracy of pressure-derived measured depth relative to an Earth-fixed datum. Each of these effects can be corrected to a varying extent, for instance by using astronomical tidal predictions to correct for tides, however some effects may be difficult or expensive to measure.

III. Approach

Our approach to real-time navigation avoids relying on compass calibration alone by applying an additional correction derived from SLAM data collected in situ, away from magnetic disturbances caused by the ship. A reasonable starting calibration (e.g., following the manufacturer's recommended procedure) is still necessary both to collect the data we use to derive the additional correction and to ensure the additional correction is small so that perturbations in pitch and roll do not result in significant heading errors.

A. Navigation Check Dive

Prior to commencing survey operations on a campaign we run a dive designed to validate navigation in general and specifically to identify compass calibration problems. Figure 4 shows tracklines from this navigation check dive as executed at the start of the Scott Reef campaign. Reciprocal legs at several headings spaced evenly around the compass rose effectively sample the distortion when compared with headings derived from the SLAM solution. True north is unobservable from the relative visual constraints and these comparisons provide a relative distortion only.

The wisdom of using the SLAM-derived headings as groundtruth may be questioned on the basis that the SLAM estimates depend in part on compass heading. To counter this effect the navigation check dive includes a regular grid which serves to constrain the arms of the star pattern relative to one another. In combination with an artificially large heading measurement noise, the constraints provided by these loop closures overwhelm compass distortion.

B. Compass Correction

We have used the relative transformations between vehicle poses estimated by the SLAM solution and compared these to the relative headings according to the compass measurements. If we compare the image-based heading to the compass heading we observe that the difference $(h_{im} - h_{nav})$ has a periodic nature as shown in Figure 4. Assuming that this distortion is consistent over the timescale of a campaign, we can compute a correction to be applied to the compass observations prior to their incorporation into the filter. This correction does not guarantee that the compass North will correspond to true North but attempts to make changes in heading consistent throughout the 360^o. We describe the correction as a truncated Fourier series and solve for it via linear least squares.

$$\Delta h_c(h_{nav}) = a_0 + \sum_{k=1}^{3} a_k cos(kh_{nav}) + b_k sin(kh_{nav}) \quad (5)$$

For small corrections the terms in this equation have physical interpretations in terms of the coefficients of hard and soft iron distortion in (4) and truncation at the second or third harmonic is typical [18].

Given multiple heading estimates based on the SLAM solution h_{im} and the corresponding compass measurement h_{nav} we form a system of equations

$$\mathbf{A}\mathbf{x} = \mathbf{b} \quad (6)$$

where

$$\mathbf{A} = \begin{bmatrix} 1 & cos(h_{nav_1}) & sin(h_{nav_1}) & \dots & sin(3h_{nav_1}) \\ 1 & cos(h_{nav_2}) & sin(h_{nav_2}) & \dots & sin(3h_{nav_2}) \\ & & & \vdots & \\ 1 & cos(h_{nav_N}) & sin(h_{nav_N}) & \dots & sin(3h_{nav_N}) \end{bmatrix}$$

$$\mathbf{x} = \begin{bmatrix} a_0 & a_1 & b_1 & \dots & b_3 \end{bmatrix}^T$$

$$\mathbf{b} = \begin{bmatrix} h_{im_1} - h_{nav_1} & \dots & h_{im_N} - h_{nav_N} \end{bmatrix}^T$$

and solve for the vector of coefficients $\mathbf{x}$.

Figure 5(a) illustrates the results of this procedure. The relative distortion as a function of measured heading is captured well by the Fourier series; however, the DC offset is effectively arbitrary. While a constant offset will not cause 'accordion' and 'figure 8' distortions of the type that confound full coverage optical surveys, an offset can result in unintended survey placement if the vehicle must first transit to reach the survey area. To avoid this problem, we compared the course-made-good from dead-reckoning versus pre- and post-dive GPS fixes on several multi-kilometer subsea transits that were also part of the Scott Reef campaign. The difference between the course-made-good computed in either case represents the distortion at the heading reported by the compass so long as the reported heading remains approximately constant over the duration of the transit. Figure 5(b) shows the final compass correction curve after least-squares determination of the DC offset. We did not utilize the GPS course-made-good data to refine the shape

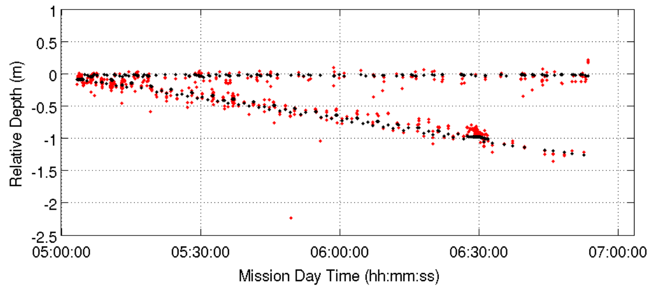

Fig. 6. The difference (red) between pressure derived depth and the vertical component of visually-derived relative pose from overlapping stereo images, and expected differences (black) from an astronomical tide prediction. Each point is plotted at the time the second image was taken. The tidal signal is visible in the line of points trending away the x-axis and corresponding to temporally distant SLAM loop closures.

of the correction, but the figure indicates consistency with the SLAM-derived correction.

C. Depth Correction

We also employ visual relative pose data to validate corrections applied to pressure-derived depth and characterise residual error. The vertical component of relative pose at loop closures identified by the SLAM result provides a measure of the change in apparent depth between reobservations. Whereas for compass correction we rely on the SLAM result as a kind of groundtruth, for validating an externally supplied correction, the SLAM result is necessary only to identify loop closures. The visual constraints can then be used directly. Figure 6 shows relative depth measurements compared with an astronomical tide prediction[1] for an AUV dive at Scott Reef. The data confirm the validity of the astronomical tide prediction as a correction to measured pressure for this data set and indicate O(0.1 m) residual errors.

IV. Field Results

The primary objective of our fieldwork at Scott Reef was to describe biological assemblages associated with coral reef systems beyond SCUBA depths. The deeper water Scott Reef habitats provide a large-scale example of the mesophotic reef habitats that occur throughout the Oceanic Shoals bioregion [20]. The South Scott Reef lagoon covers 300 km^2 and is the largest area of this type observed on a single reef system in the NW region. Understanding the nature and dynamics of these deeper water areas will not only better describe the true extent of Australia's tropical reef resources, but will contribute to a broader understanding of the overall resilience of coral reefs in the NW region [20]. During the last decade a few surveys using simple towed video and small ROVs have begun to be used to survey the deeper South Scott Reef lagoon [21]. The initial habitat maps derived from these surveys suffer from the coarse interpolation used to join a limited number of survey points. The quality of the video used has also severely restricted the taxonomic resolution

[1]Courtesy of Geoscience Australia

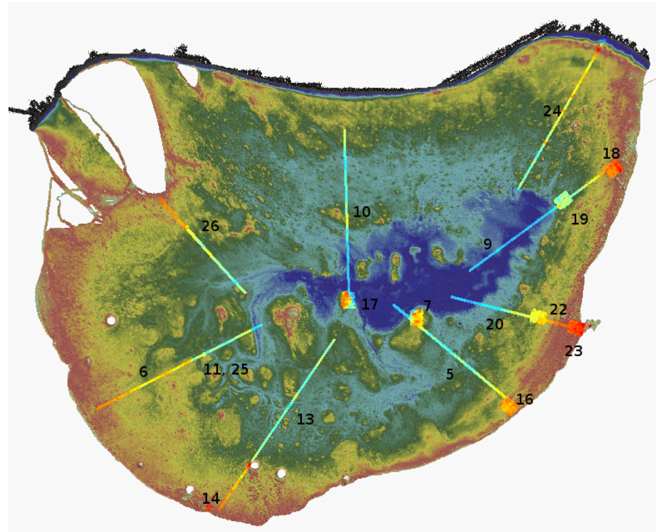

Fig. 7. Dive profiles flown by the vehicle during the course of the cruise. Full coverage optical survey patterns were undertaken on dives 11, 14, 25 and 26. The background image is first-pass 4 m resolution multibeam bathymetry generated during the cruise (image courtesy of Geoscience Australia). The AUV dive profiles are overlaid on top of the bathymetry and are colour coded by inferred depth of seafloor.

possible, precluding accurate assessment of species distributions and has provided limited information for monitoring purposes.

The sampling program involved 24 hour operations comprising deployments of the AUV and a towed video system during the day followed by swath mapping of the South Scott Lagoon during the night. The twice daily AUV missions each lasted between 3 to 6 hours in water depths from 20 to 110 m during both spring and neap tide cycles. In total, the AUV missions covered ∼110 km of habitat at South Scott Reef with the AUV collecting high resolution stereo pairs at 1 Hz from an altitude of 2 m. The AUV conducted a total of 19 science missions including combinations of straight line transects, open grids, and full coverage surveys. Figure 7 shows the dive profiles overlaid on the multibeam bathymetry collected during the trip by Geoscience Australia.

A. Navigation Improvement

Demonstrating the ability to conduct full coverage surveys was a major engineering objective of the cruise. In collaboration with the Australian Institute for Marine Science (AMIS) we will return to these sites regularly over the next few years with the aim of generating a record of change in the deep reef benthos. Figure 8 shows an example of a full coverage dive undertaken in a deep water area of the lagoon. This particular dive was designed to survey an interface between dense foliose coral cover and sand identified in one of the previous long transects. The vehicle was programmed to descend to the seafloor, complete a 100 m leg followed by a full coverage grid of 75 m x 50 m with 1 m spacing between legs.

Figure 8 shows the estimated vehicle trajectories for the full SLAM solution with the compass correction applied

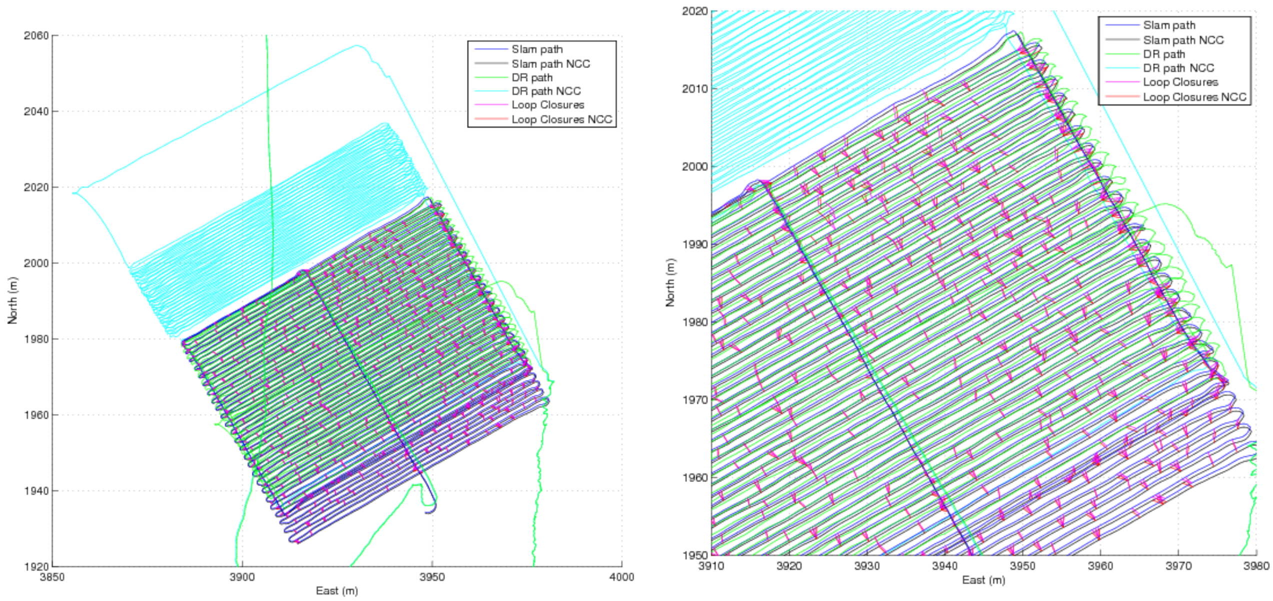

(a)

(b)

Fig. 8. (a) Estimated vehicle trajectories for the full SLAM solution with and without the compass correction applied. (b) A closer view of the survey pattern illustrating the similarity of the two SLAM solutions and showing that the dead reckoned estimate with compass correction applied is within approximately 10 m of the SLAM estimate even after in excess of 5 km of travel and over one hundred 180^o turns.

(blue), the full SLAM solution with no compass correction (black), the dead reckoned path with compass correction (green) and the dead reckoned path without the compass correction (cyan). The SLAM loop closures are shown for the case of SLAM with compass correction (magenta) and without compass correction (red). Both SLAM solutions are consistent in this case. The dead reckoned estimates, on the other hand differ significantly. In the case when the compass observations are not corrected, the filter estimates that the vehicle is proceeding in the opposite direction to the desired survey pattern. The estimated vehicle trajectory with the correction applied is significantly closer to the final SLAM solution. Note that the strong constraints imposed by the relative pose observations provided by the visual features are sufficient to yield a consistent solution even when the compass observations feature significant biases. Figure 9 shows the position innovations for the observations received from GPS at the start and end of the dive. As can be seen, the innovation on completion of the dive is consistent with the innovation gates for the SLAM filters. The dead reckoning estimates, on the other hand, show large innovations at the end of the dive, particularly when the compass correction is not applied. Figure 10 shows the resulting 3D reconstruction of the survey area and associated fine scale multibeam bathymetry collected by the vehicle.

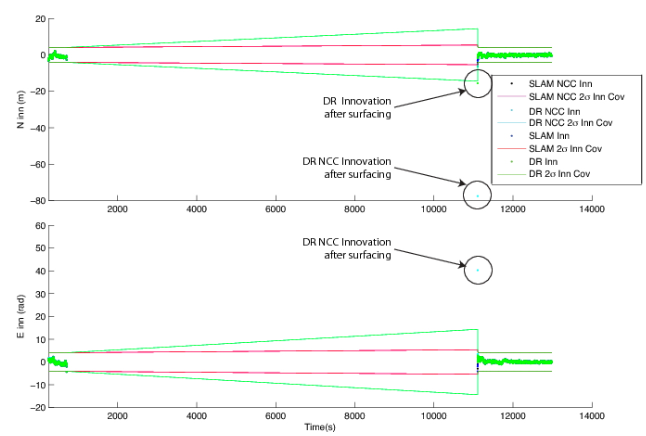

Fig. 9. Position innovations and associated 2σ innovation covariances logged by the SLAM filters for GPS observations. All of the filters have consistent innovations prior to the start of the dive. At the end of the dive, when the vehicle resurfaces, the two dead reckoned solutions (with and without the compass correction applied to the heading observations) show large innovations - on the order of 10m when the compass correction is applied and nearly 90 m without. The two SLAM solutions, on the other hand, show an innovation of less than five meters after more than 3 hours of survey time.

B. Visual Consistency of Seafloor Reconstructions

The scientific use and understanding of benthic habitat surveys consisting of thousands of images can benefit from user-friendly visualization as mosaics or 3D texture-mapped reconstructions. Both of these representations require an emphasis on visual consistency to be effective [22]. Depth errors due to uncompensated pressure measurements can produce visual artifacts such as sharp steps when revisiting a patch of seafloor. Moreover, quantitative interpretation of 3D reconstructions in terms of biologically important habitat characteristics like rugosity, slope and aspect may suffer from false structure induced by depth errors. Figure 11 illustrates how depth errors can produce false structure where images overlap. Compensating measured depth with astronomical

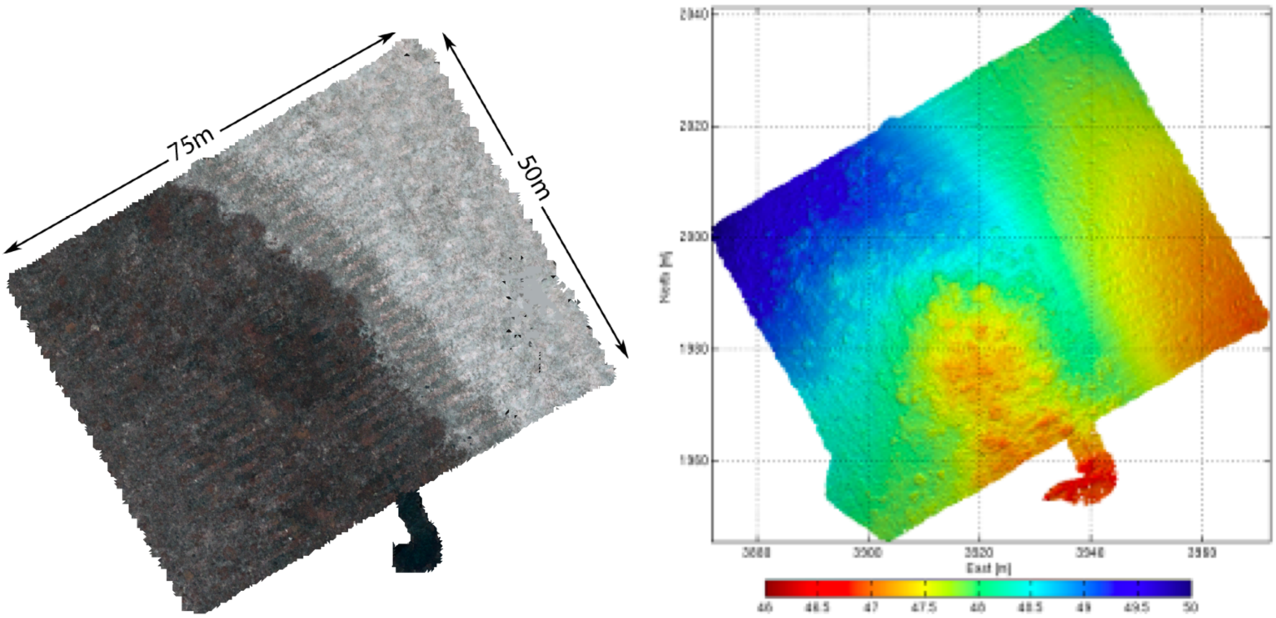

(a) (b)

Fig. 10. (a) A 3D reconstruction of the dense survey undertaken with the corrected compass calibration (b) The bathymetry collected using the vehicle's multibeam sonar.

tide data eliminated the false structure in this case.

V. Conclusion

In this paper we showed how visually-augmented SLAM results generated in post-processing can be used to (1) improve real-time dead-reckoned navigation for vehicles equipped with mid-range navigation suites dependent on magnetic compasses, and (2) to validate the accuracy of depth corrections. Our efforts were motivated by the need to collect full coverage grid surveys of the benthos for ecological monitoring purposes. We successfully demonstrated this capability with a large 50 m by 75 m composite image of deep reef during field work at Scott Reef, WA.

We continue to refine the techniques presented here by investigating a bundle adjustment approach to identifying compass distortion so as to eliminate partial dependence of SLAM groundtruth on the compass itself. We also plan to alter the navigation check dive to include a relatively long subsea transit followed by a surface GPS fix in order to identify both the relative compass distortion and the absolute offset to true north in a single dive.

Acknowledgment

This work is supported by the ARC Centre of Excellence programme, funded by the Australian Research Council (ARC) and the New South Wales State Government and the Integrated Marine Observing System (IMOS) through the DIISR National Collaborative Research Infrastructure Scheme. The authors would also like to thank the Australian Institute for Marine Science for making ship time available to support this study. The crew of the R/V Solander were instrumental in facilitating successful deployment and recovery of the AUV. The ship-borne multibeam sonar data were collected, processed and gridded to produce DEMs by Geoscience Australia. Thanks also to Dr. Mike Sexton and Shoaib Burq from Geoscience Australia for collecting the multibeam data and making it available. We also acknowledge the help of all those who have contributed to the development and operation of the AUV, including Duncan Mercer, George Powell, Matthew Johnson-Roberson, Ian Mahon, Stephen Barkby, Ritesh Lal, Paul Rigby, Jeremy Randle, Bruce Crundwell and the late Alan Trinder.

References

[1] C. Kunz, C. Murphy, H. Singh, C. Willis, R. Sohn, S. Singh, T. Sato, C. Roman, K. Nakamura, M. Jakuba, R. Eustice, R. Camilli, and J. Bailey, "Toward extraplanetary under-ice exploration: Robotic steps in the Arctic," *Journal of Field Robotics*, vol. 26, no. 4, Apr. 2009, special Issue on Space Robotics, Part 2.

[2] R. Marthiniussen, K. Vestgard, R. Klepaker, and N. Storkersen, "HUGIN-AUV concept and operational experiences to date," in *OCEANS '04. MTTS/IEEE TECHNO-OCEAN '04*, vol. 2, 2004, pp. 846–850 Vol.2.

[3] D. R. Yoerger, M. Jakuba, A. M. Bradley, and B. Bingham, "Techniques for deep sea near bottom survey using an autonomous underwater vehicle," *International Journal of Robotics Research*, vol. 26, no. 1, pp. 41–54, Jan. 2007.

[4] S. A. Y. and G. G. G., "A coastal current in winter: Autonomous underwater vehicle observations of the coastal current east of cape cod," *J. Geophys. Res.*, vol. 113, p. C07030, 2008.

[5] I. Robbins, G. Kirkpatrick, S. Blackwell, J. Hillier, C. Knight, and M. Moline, "Improved monitoring of HABs using autonomous underwater vehicles (AUV)," *Harmful Algae*, vol. 5, no. 6, pp. 749–761, 2006.

[6] M. J. Caruso, "Applications of magnetic sensors for low cost compass systems," in *Position Location and Navigation Symposium, IEEE 2000*, Mar. 2000, pp. 177–184.

[7] R. Eustice, H. Singh, J. Leonard, and M. Walter, "Visually mapping the RMS Titanic: Conservative covariance estimates for SLAM information filters," *The International Journal of Robotics Research*, 2006.

[8] I. Mahon, S. Williams, O. Pizarro, and M. Johnson-Roberson, “Efficient view-based SLAM using visual loop closures,” *Robotics, IEEE Transactions on*, vol. 24, pp. 1002 – 1014, 2008.

[9] R. Eustice, O. Pizarro, and H. Singh, “Visually augmented navigation for autonomous underwater vehicles,” *Oceanic Engineering, IEEE Journal of*, vol. 33, pp. 103 – 122, 2008.

[10] O. Pizarro, R. M. Eustice, and H. Singh, “Large area 3-d reconstructions from underwater optical surveys,” *IEEE Journal of Oceanic Engineering*, vol. 34, no. 2, pp. 150–169, 2009.

[11] D. Lowe, “Distinctive image features from scale-invariant keypoints,” *International Journal of Computer Vision*, vol. 60, pp. 91–110, 2004.

[12] R. Hartley and A. Zisserman, *Multiple View Geometry in Computer Vision*. Cambridge University Press, 2000.

[13] I. Mahon, “Vision-based navigation for autonomous underwater vehicles,” Ph.D. dissertation, University of Sydney, 2008.

[14] M. Dissanayake, P. Newman, S. Clark, H. Durrant-Whyte, and M. Csobra, “A solution to the simultaneous localization and map building (slam) problem.” in *IEEE Transactions on Robotics and Automation*, vol. 17(3), 2001, pp. 229–241.

[15] H. Durrant-whyte and T. Bailey, “Simultaneous localisation and mapping (SLAM): Part I the essential algorithms,” *Robotics and Automation Magazine*, vol. 13, pp. 99–110, 2006.

[16] I. Mahon, S. B. Williams, O. Pizarro, and M. Johnson-Roberson, “Efficient view-based SLAM using visual loop closures,” *IEEE Transactions on Robotics and Automation*, vol. 24, no. 5, pp. 1002–1014, Oct. 2008.

[17] R. Eustice, H. Singh, J. Leonard, and M. Walter., “Visually mapping the RMS Titanic: conservative covariance estimates for SLAM information filters,” *Intl. J. Robotics Research*, vol. 25, no. 12, pp. 1223–1242, 2006.

[18] A. Hine, *Magnetic Compasses and Magnetometers*. London: Adam Hilger Ltd., 1968.

[19] J. C. Kinsey, R. M. Eustice, and L. L. Whitcomb, “A survey of underwater vehicle navigation: Recent advances and new challenges,” in *IFAC Conference of Manoeuvering and Control of Marine Craft*, Lisbon, Portugal, Sept. 2006.

[20] A. J. Heyward, “Seduced by SCUBA? : depth provides refuge for coral reefs,” in *Australian Coral Reef Society, 83rd annual conference, east meets west: science and management of Australia’s coral reefs*, Fremantle, Western Australia, Oct. 2007.

[21] A. Heyward, M. Rees, and L. Smith, “Scott reef deeper lagoon habitat preview and recommendations for further assessment,” Australian Institute of Marine Science, Tech. Rep., 1999.

[22] M. Johnson-Roberson, O. Pizarro, S. Williams, and I. Mahon, “Generation and visualization of large-scale three-dimensional reconstructions from underwater robotic surveys,” *Journal of Field Robotics*, vol. 27, no. 1, pp. 21–51, 2010.

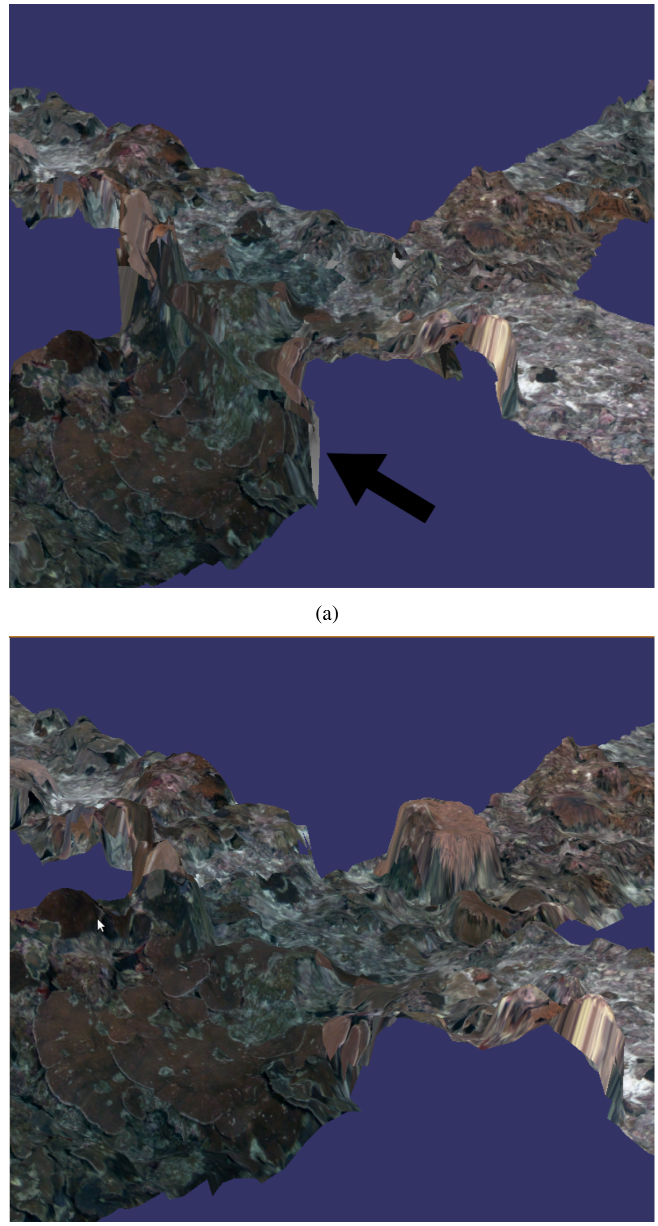

(a)

(b)

Fig. 11. Three-dimensional seafloor reconstruction of a loop closure: (a) without astronomical tide correction; (b) with astronomical tide correction. Without compensating for astronomical tide, the reconstruction contains false relief in the form of a steep wall. On temporally distant loop closures like this one, where the vehicle observed the same patch of seafloor after an interval of more than an hour, the false structure is pronounced (arrow).